Technical and Ecological Limits of 2.45-GHz Wireless Power Transfer for Battery-Less Sensors

Marco Gonzalez, *Student Member, IEEE,* Pengcheng Xu, *Member, IEEE,* Rémi Dekimpe, *Student Member, IEEE,* Maxime Schramme, *Student Member, IEEE,* Ivan Stupia, *Member, IEEE,* Thibault Pirson, and David Bol, *Senior Member, IEEE*

***Abstract*—Wireless power transfer (WPT) is a possible alternative to batteries for supplying smart sensors. It is often described as "greener" because it avoids the use of batteries. However, this claim usually lacks the proper assessment of the environmental impacts of WPT and is particularly questionable given the poor efficiency of wirelessly transmitting power over a few meters of distance. In this paper, we design and thoroughly optimize a complete state-of-the-art WPT system and compare it to an equivalent battery-powered solution to assess whether it effectively represents an eco-friendly alternative. The proposed WPT system is a 2.45-GHz simultaneous wireless information and power transfer (SWIPT) system with beamforming and a high peak-to-average power ratio waveform for supplying a battery-less passive infrared sensor for room occupancy tracking. The final prototype of the smart sensor consumes 4 µW and can operate in steady state at 5 m from the remote power head with an overall power transfer efficiency of 17 µW/W and can cold-start at 3.5 m. We carry out a life-cycle assessment (LCA) of the environmental impacts through four indicators, i.e., primary energy demand, global warming potential, terrestrial ecotoxicity, and freshwater consumption. Results show that for a 10-year lifetime, the WPT alternative has at least 5.5 to 10.3× higher environmental impacts than its battery-powered equivalent. This demonstrates the importance of LCA during the design of IoT smart sensors and shows that the use of meter-range 2.45-GHz SWIPT should be limited to applications where conventional battery-powered systems cannot be used.**

***Index Terms*—Internet-of-Things, life-cycle assessment, motion detection, RF energy harvesting, room occupancy tracking, smart sensors, ultra-low-power, wireless power transfer.**

I. Introduction

As of today, billions of objects are connected to the internet under the concept of the Internet of Things (IoT) and this number will continue to grow in the upcoming years [1], [2]. This has made possible the emergence of a variety of applications in, e.g., healthcare, industries, cities, buildings, and homes. A typical application of IoT for smart buildings consists in monitoring room occupancy for surveillance or for the optimization of the building's total energy consumption through smart light control and heating, ventilation, and air conditioning (HVAC) regulation. Commercial solutions for this already exist and they operate on batteries [3] or are supplied by the building's AC electrical infrastructure [4] [5]. These solutions could be an obstacle to the adoption of such technologies in multi-story buildings because of the cost of deployment and maintenance of a high number of smart sensors.

All authors are/were with the ICTEAM institute of Université catholique de Louvain (e-mail: marco.gonzalez@uclouvain.be). Pengcheng Xu is now with Fraunhofer EMFT.

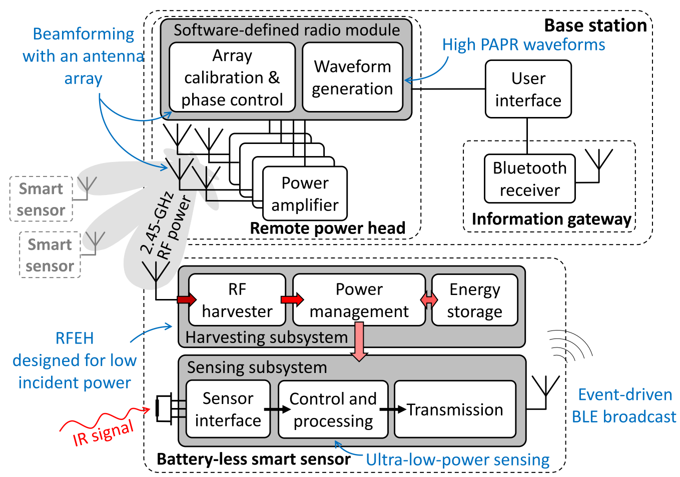

Fig. 1. Proposed system architecture. It includes several smart sensors and a shared base station, composed of the RPH and the information gateway. One of these sensors is shown in detail.

As proposed in [6], wireless power transfer (WPT) is a possible solution to overcome these limitations as the power used to supply the smart sensors is transmitted through the air from a remote power head (RPH). This removes the need for wires or batteries for the operation of the sensors, which instead harvest the incident RF energy. It is often referred to as a green alternative in grey and scientific literature because it replaces batteries [7]–[9]. Nevertheless, the low efficiency of this technology, mainly caused by the path loss due to wave propagation, restricts the range of applications to those with simple tasks that need only very low power to complete. Therefore, an important trade-off appears. On the one hand, the distance between the sensors and the RPH can be reduced to increase the harvested power, resulting in the ability to handle more complicated applications. An example is the real-time monitoring of an engine done in [10], where the sensors are supplied with a 2.45-GHz WPT and are separated by only 54 cm from the RPH. There are mainly two disadvantages in this case. Either the spatial coverage of the sensors is severely reduced, or the number of RPHs must increase to supply all the sensors. Both options limit the applications for which the system could represent a technically viable alternative. On the other hand, the distance can be maximized to have the minimal number of RPHs for the desired range of the sensors by reducing the power consumption of the smart sensor, at the cost of limited applicative functionality such as low-rate data

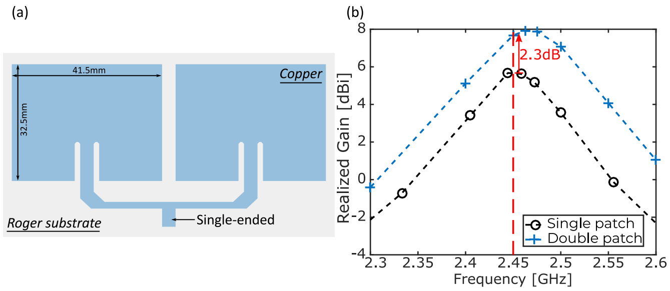

Fig. 2. Antenna pattern (a) and realized gain (b) of a dual single-ended rectangular patch antenna. The realized gain is 2.3 dB higher than that of a single-patch antenna at 2.45 GHz.

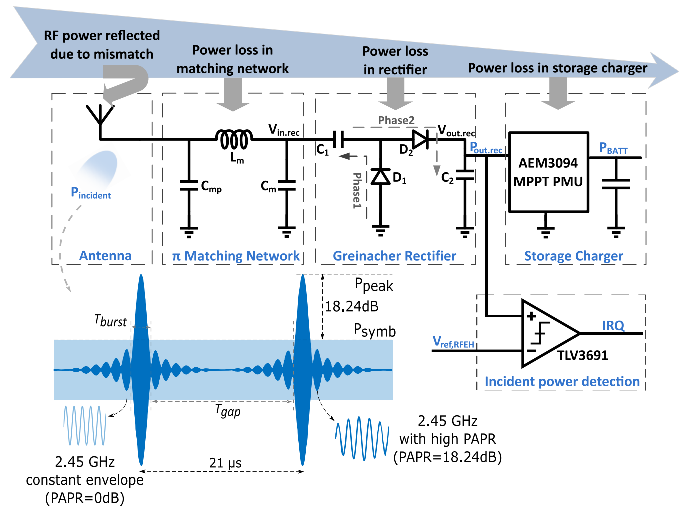

Fig. 3. RF energy harvesting subsystem with high-PAPR input waveform showing the automatic detection of power at the output of the rectifier.

logging. This approach is illustrated in [11], where a simple temperature and humidity monitoring system can operate at 17 m from the RPH which sends power at 868 MHz.

Simultaneous wireless information and power transfer (SWIPT) is a popular research concept that has been studied both at sub-GHz frequencies [12], [13] and at 2.4 GHz [10], [14]. In this paper, we focus on 2.4-GHz WPT to supply an application with intermediate complexity and WPT range, where we aim at an always-on presence detection for room occupancy tracking through the design and optimization of a WPT system with a battery-less infrared motion detector and Bluetooth Low Energy (BLE) communication. This design serves as a base for the study of the technical limits of the WPT technology. We further evaluate if it is actually an eco-friendly alternative to battery-powered smart sensors by conducting a life-cycle assessment (LCA) of the environmental impacts.

This paper is structured as follows. Section II describes the system architecture. Section III discusses the wireless power transmission and RF energy harvesting to evaluate the supply link budget of the system and estimate the total available power for the operation of the smart sensor, whose optimization is described in Section IV. The problem of the cold start of the smart sensor and the global system performance are presented in Section V. Finally, LCA results are provided in Section VI.

II. System Architecture

The proposed SWIPT system is composed of three parts, as shown in Fig. 1. The first is the RPH, which transmits the RF power to the smart sensor. The second is the smart sensor, here a battery-less infrared occupancy sensor. Finally, the third is the information gateway, which communicates with the smart sensor using BLE to track the changes in occupancy in the room.

The smart sensor is composed of two subsystems: the harvesting and the sensing subsystems. The harvesting subsystem includes the Radio-Frequency Energy Harvester (RFEH) which rectifies the RF energy received with a patch antenna to an unregulated DC voltage using a Greinacher rectifier built with discrete components. The AEM30940 power management unit (PMU) from e-peas [15] generates a regulated supply voltage for the sensing subsystem from the unregulated DC voltage. Additionally, a capacitor is connected to the PMU to store the excess energy that is not immediately used by the sensing subsystem and to provide the excess energy for its moments of peak consumption. The sensing subsystem contains a passive infrared (PIR) transducer ZRE200GE from Zilog [16]. It is interfaced with an analog front-end (AFE), built with discrete components, which amplifies and filters the transducer signal. Finally, a microcontroller unit (MCU) controls the smart sensor and transmits the information to the gateway with its embedded Bluetooth 5 transceiver, compatible with BLE.

The smart sensor is powered remotely from a software-defined radio, implemented with National Instruments USRP-2944 devices [17], with 2.45-GHz WPT using a high peak-to-average power ratio (PAPR) custom waveform which enables a higher harvesting efficiency on the smart sensor at a lower incident power [18]. The RPH further embeds four TPQ9111 power amplifiers from Triquint [19], each feeding an antenna of the array that creates a beam in the direction of the smart sensor.

Finally, the information gateway, composed mainly of a Bluetooth transceiver, communicates with the smart sensor and for demonstration purposes controls the lighting of the room by switching on and off an electrical relay.

III. Wireless Power Transfer

The applicative functionality and the spatial coverage of the smart sensor are directly linked to the power available for its operation. It can be estimated from the performance of the RFEH and the RPH. The design of these blocks as well as the supply link budget are discussed in the following subsections to derive the power consumption target of the smart sensor.

A. RF Energy Harvesting

In far-field or radiative WPT, power is transferred through beams of electromagnetic radiation at radio frequency, such as the license-free 2.45 GHz. The receiver part of far-field WPT is the RF energy harvesting subsystem of the smart sensor. As depicted in Fig. 1, it collects the RF power sent by an RPH, and then converts and regulates the RF power into a stable voltage for supplying the sensing subsystem.

For improving the realized gain of the receiving antenna and thus reducing the RF path loss, a dual rectangular patch

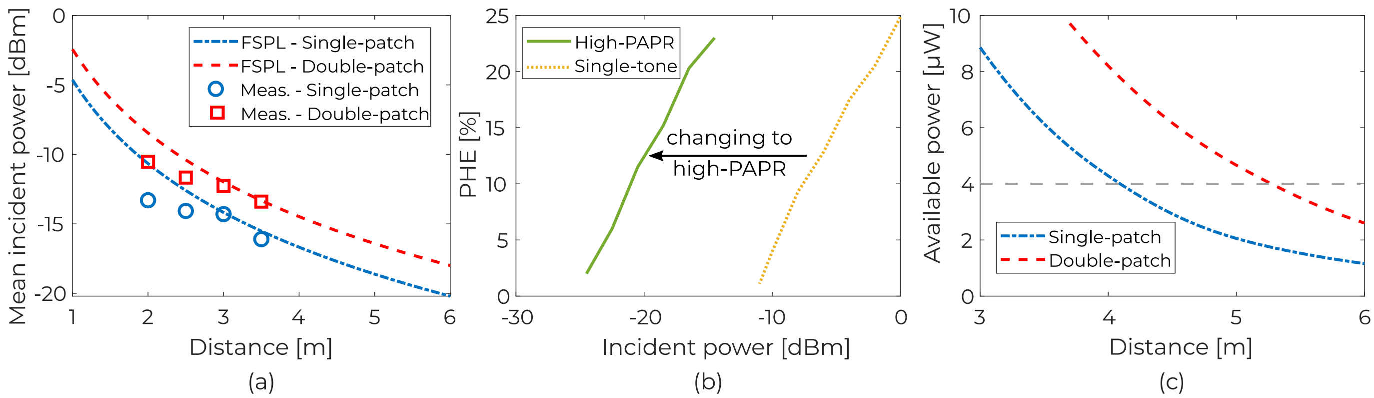

Fig. 4. (a) Average input power versus distance with single- and double-patch antenna, at 2.45 GHz and considering perfect beamforming and free-space path loss (FSPL). (b) Measured power harvesting efficiency (PHE) of the Greinacher rectifier including the PMU. (c) Total harvested power available for the operation of the smart sensor.

antenna was designed as depicted in Fig. 2(a). Each patch antenna has a size of 32.5 mm×41.5 mm. The feed lines of the two antennas are connected to have a single-ended output. Here, we used the Roger 4003C process featuring lower RF power losses than the FP4 material. Fig. 2(b) shows the realized gain, which increases around 2.3 dB for the double-patch antenna compared to the single-patch antenna at the nominal frequency.

As depicted in Fig. 3, after the receiving antenna, the π matching network converts the input impedance of the rectifier to the antenna impedance to avoid RF power reflection due to impedance mismatch. It was designed with parasitic-aware sizing, as explained in [6]. A Greinacher rectifier composed of Schottky diodes, as the one used in [6], performs the AC/DC conversion. As increasing the number of stages in the rectifier only increases its output voltage at a fixed efficiency [20], a single stage was selected to keep the output voltage below the maximum 5 V that the PMU can withstand, even during the power bursts of the high-PAPR waveform. In this work, the AEM3094 PMU is used for maximum power point tracking (MPPT) [15] to improve the power harvesting efficiency (PHE). This efficiency is defined as the ratio between the harvested DC output power ($P_{\text{EH,out}}$) and the incident RF power (P_{incident}) at the antenna [6], [21]:

$$\text{PHE}(P_{\text{incident}}) = \frac{P_{\text{EH,out}}}{P_{\text{incident}}}. \quad (1)$$

Each stage of the RFEH contributes to the power loss, as illustrated in Fig. 3, reducing the harvested power used to supply the IoT smart sensor and degrading the PHE. The PHE of 2.45-GHz RFEHs is high only at high levels of incident power [21], mainly because the equivalent input impedance of the rectifier increases exponentially at low levels [18]. However, the path loss over the wireless link significantly degrades the level of incident power P_{incident}, especially at the high operational frequency used, 2.45 GHz. To improve the PHE at low incident power, and thus increase the achievable distance between the RFEH and the RPH, a high-PAPR waveform is used to contract the low average RF power to short high-power bursts [18]. A high-PAPR waveform can be generated through the superposition of different tones where the peak power level can be controlled by introducing a phase offset between the tones. We generate the high-PAPR WPT waveform by using 64 tones, modulated with binary phase-shift keying, for a total bandwidth of 3-MHz fitted in two 2-MHz adjacent BLE channels, that we allocate to WPT. Fig. 3 compares the single-tone waveform in light blue with the 18.24-dB PAPR waveform in dark blue. The 21 μs of separation between power peaks are divided in 0.65 μs of the high power burst (T_{burst}) and 20.35 μs of gap (T_{gap}). The PHE is significantly improved at low P_{incident} as depicted in Fig. 4(b), reaching 12.5 % at −20 dBm, which is comparable to state-of-the-art designs such as [22].

B. Wireless Power Transmission

Phased antenna arrays are collections of antenna elements capable of beamforming, i.e., radiating electromagnetic energy towards desired locations by constructively combining individual signals while destructively interfering in other directions to minimize side lobes. To counteract the detrimental effect of the path loss on the power transfer efficiency, the proposed RPH embeds a phased array of four elements whose configuration is adapted on the fly to maximize the power received by the smart sensor.

Even though beamforming requires only limited resources, the main technical requirement to compute the beamforming coefficients is the assumption of Channel State Information (CSI) knowledge at the transmitter side. This is usually obtained by making use of known pilot symbols, which requires the estimation of the CSI at the smart sensor and a feedback link to the RPH. This procedure may be problematic in RF-supplied smart sensors since it requires enough energy for the execution of a channel estimation algorithm as well as an additional dedicated transmission to communicate the channel coefficients to the RPH. An interesting alternative to overcome this obstacle as a trade-off between the performance improvement of beamforming and its complexity overhead consists in the exploitation of the channel reciprocity theorem. Channel reciprocity allows the estimation of CSI directly at the RPH from a beacon transmitted by the smart sensor. This is possible in SWIPT systems under the condition of sharing the available resources through a time division duplexing (TDD) protocol.

The TDD protocol was implemented as shown in Fig. 5. The power transfer is structured in frames of 100 ms. When the controller schedules a beacon transmission, the RPH stops the power frame transmission. Therefore, the voltage at the

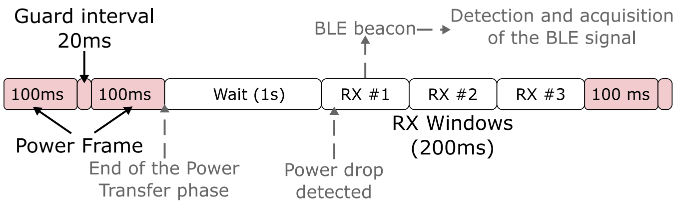

Fig. 5. Time Division Duplexing protocol for the energy and data transfer between the RPH and the smart sensor.

RFEH rectifier output starts decreasing and the availability of the frequency resource for data transmission is identified by introducing an incident-power detector in the smart sensor. As shown in Fig. 3, this detector is implemented with a comparator that generates an IRQ to the MCU in case the output of the RFEH rectifier goes below a certain voltage reference generated in the resistive ladder of the AFE, shown in Fig. 11. The TLV3691 comparator [23] was chosen because of its ultra-low power consumption. When the drop of the incident power is detected, it means that the channel is available for transmitting a beacon for CSI evaluation. When catching this IRQ, the MCU thus transmits a BLE beacon with a different payload than for motion detection. In order to correctly estimate the CSI with a decent SNR, the RPH cannot transmit power when receiving the beacon. Therefore, during the transmission of the BLE beacon, the RPH scans three RX windows of 200 ms to localize the BLE signal within the time interval available for beacon transmission. Since BLE uses constant-envelope GFSK signals, a simple yet effective solution to sense the presence of a beacon consists in finding the locations of any pair of signal level-crossings within the pre-determined RX windows. When a rising edge and a subsequent falling edge are detected, the time interval between the two events is then compared with the expected length of the BLE signal to minimize false alarm events. If the distance between the two edges is compatible with the BLE beacon, the samples are acquired, their covariance matrix is filtered through the steering signature vector of the antenna array to extract the signal impinging directions and the beamforming coefficients are finally obtained as the complex conjugate of the first eigenvector of the covariance matrix [24].

The impact of the proposed beamforming strategy was tested in a dynamic environment and in the presence of multiple reflections and small obstacles. In order to evaluate the benefits of the proposed strategy on the power transfer efficiency, the RPH and the smart sensor were deployed at the UCLouvain premises during working hours, and the incident power at the harvester antenna was measured with and without beamforming. Two different antenna designs have been tested, namely single-patch and dual-patch antennas (see Section III-A for more details). Fig. 6 reports the average received power for six different random positions of the harvester in a range between 2 and 3 m from the RPH. The proposed beamforming procedure increases the average received power by 1.3 to 20.6 dB for the different positions when using the dual-patch antenna.

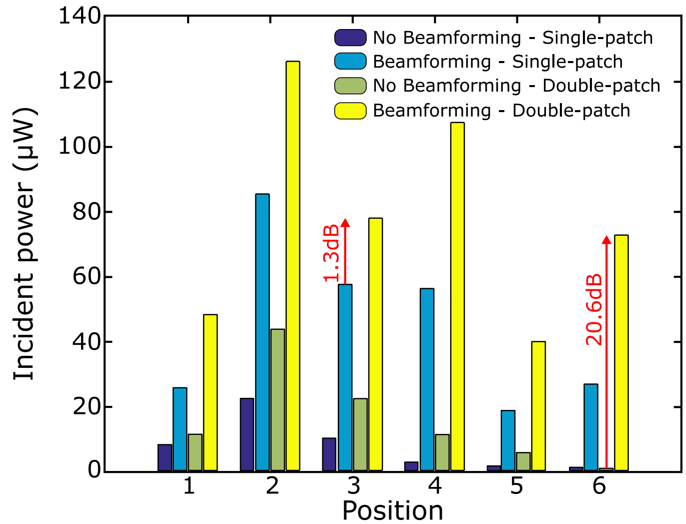

Fig. 6. Average received power by the RFEH at six random positions in a range between 2 and 3 m from the RPH in an office environment for a transmitted power of 15 dBm.

C. Supply Link Budget

The total power available for the sensing subsystem can be estimated from the performance of the different parts of the WPT system.

First, a portion of the power transmitted by the RPH is lost due to the propagation through the wireless channel. Assuming perfect beamforming by the RPH and a free-space propagation, the power received by the smart sensor in dBm is derived from the Friis transmission equation as a function of the distance:

$$P_{\text{incident}} = P_{\text{TX,out}} + G_{\text{T}} + G_{\text{A}} + G_{\text{R}} - 20\log\left(\frac{4\pi f d}{c}\right), \quad (2)$$

where $P_{\text{TX,out}}$ is the transmitted power, 15 dBm, corresponding to the maximum allowed power by the EIRP regulations; G_{T} is the antenna gain of the transmitter, 3 dBi, derived from their physical dimensions; G_{A} is the array gain at the transmitter, 12 dB, corresponding to a 4-antenna array; G_{R} is the antenna gain of the receiver, equal to 5.7 or 7.9 dBi for the single- and double-patch antenna, respectively; c, f, and d are the speed of light, the frequency of the wave and the distance between the RPH and the smart sensor, respectively. This theoretical calculation is compared to measurements in an office environment in Fig. 4(a). For each measurement at each distance, the receiving antenna was oriented toward the RPH and the beamforming coefficients were estimated again to adapt to the new conditions. As expected, the experimental results do not match the simplified model of free-space propagation, mainly because of the obstacles present in an office environment which create multiple paths of propagation that decrease the mean received power. However, at distances greater than 3 m, the beamforming is able to leverage these multiple paths to compensate for the adverse propagation conditions and allows to receive a level of power close to what was theoretically estimated.

The received signal is then rectified by the RFEH and the resulting DC voltage is regulated by the PMU, providing the supply that will be used by the smart sensor for its operation. The efficiency of these two operations is included in the PHE depicted in Fig. 4(b) as a function of the incident power, and

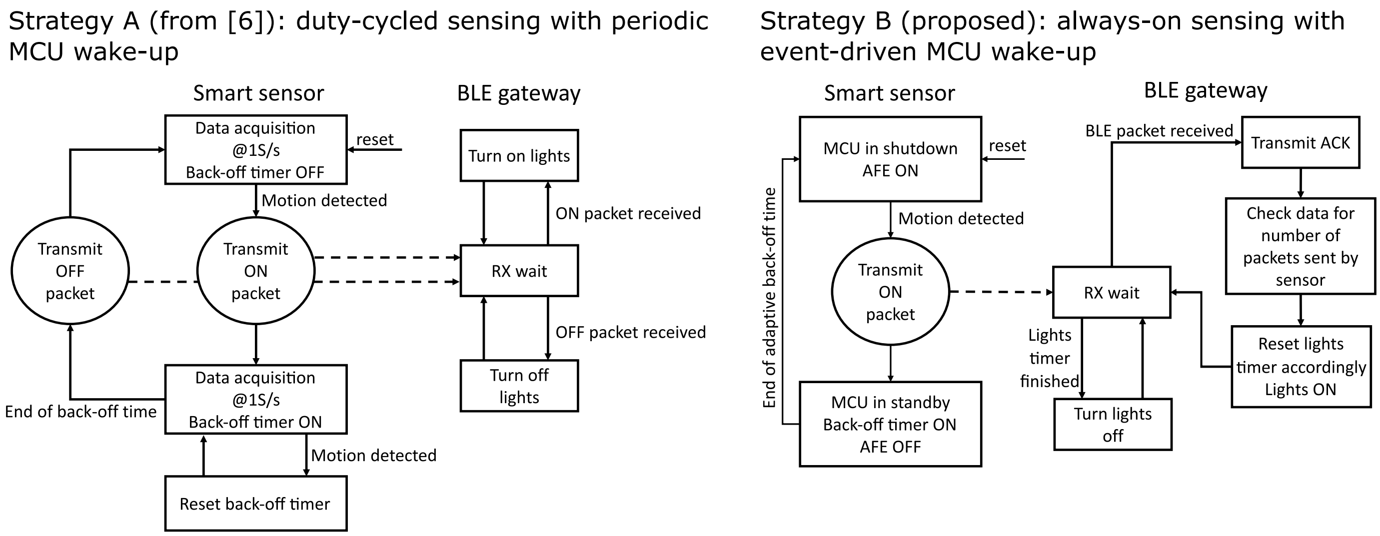

Fig. 7. Flowcharts of the communication schemes between the information gateway and the smart sensor.

therefore of the distance [18].

The total power available for the operation of the smart sensor, i.e., the harvested power, can be estimated using (1). The result is shown in Fig. 4(c). It can be noticed that the power consumption of the smart sensor must remain below 4 µW to enable a distance of 5 m between the RPH and the smart sensor. Unfortunately, the harvested power can only be estimated from a model because the probing of the output supply voltage introduces a prohibitive leakage at very low harvested power.

To evaluate the global performance of the system, we define the power transfer efficiency (PTE) as the ratio between the harvested power and the power consumed by the transmitter of the RPH ($P_{\text{TX,in}}$), which gives:

$$\text{PTE} = \frac{P_{\text{EH,out}}}{P_{\text{TX,in}}} = \text{PTXE} \times \text{Path Loss} \times \text{PHE}, \quad (3)$$

where PTXE is the transmitter efficiency, i.e., the ratio between $P_{\text{TX,out}}$ and $P_{\text{TX,in}}$, and path loss is the ratio between received and transmitted power that can be computed from (2).

IV. Motion Detection Strategies

In order to meet the power constraint of 4 µW for the smart sensor, special attention must be paid to the strategy used in the sensing subsystem to successfully detect a movement and alert the gateway. This is because each strategy implies a trade-off between the system latency when detecting movements and the average power consumption.

The strategy used in [6] to decrease the average power of the system combines three techniques: duty-cycled sensing with periodic MCU wake-up, event-driven communication, and the use of a back-off time, i.e., a minimal delay between two packet transmissions. This strategy results in a low latency when detecting movements, but unfortunately, the back-off time and the period of the duty-cycled sensing would both need to increase 3× to achieve the 4-µW target of power consumption, therefore greatly deteriorating the latency and thus the applicative functionality.

Let us study an alternative strategy with a simpler control from the MCU, to spend more time in sleep mode. This strategy relies on always-on sensing and event-driven MCU wake-up while keeping the back-off time and the event-driven communication done in [6].

In addition to the choice of strategy, the choice of MCU is also important as it has a great impact on the average power consumption of the system due to performance trade-offs. In the following subsections, a comparison between the CC2650 from Texas Instruments [25] used in [6] and the STM32WB55 [26] will be detailed as well as an analysis of the two aforementioned strategies in terms of average power consumption during both motion detection in absence of motion and in the worst-case scenario. The latter is the one limiting the maximum achievable distance between the smart sensor and the RPH because it sets the lower limit on the amount of power that must be harvested for stable operation.

A. Strategy A: Duty-cycled Sensing with Periodic MCU Wake-up

In [6], the CC2650 MCU from Texas Instruments [25] was used. It provided the supply voltage of the AFE via a general-purpose input/output (GPIO) pin and therefore was able to control the duty-cycling of the sensing operation to have an active time of 10 ms with a period of 1 s (1 % of duty-cycle). The rest of the time, the MCU had to enter the deepest possible sleep state with functional real-time clock (RTC), which in the case of both the CC2650 and the STM32WB55 is called standby mode.

During this motion detection stage, the system is at its minimum in power consumption, which can be computed as

$$P_{\text{detect}} = P_{\text{stdby}} + E_{\text{acq}} f_{\text{S}}, \quad (4)$$

where P_{stdby} is the standby power of the MCU, E_{acq} is the energy consumed for data acquisition including the ADC conversion energy and the AFE power integrated over its short active time, and f_{S} is the sampling frequency. This equation shows that the power consumption during motion detection can be reduced by having a lower sampling frequency, which unfortunately decreases the responsiveness of the system, and also that the power is ultimately limited by P_{stdby}.

The worst-case scenario depends on the communication scheme used to inform the gateway of the occupancy of the

TABLE I
COMPARISON OF THE PERFORMANCE OF THE MCUS.

	CC2650 [6], [25]	STM32WB55 [26] standalone	STM32WB55 [26] with AFE
Standby power (P_{stdby})	4 µW[1]	0.7 µW/1.08 µW[1]	1.09 µW
Shutdown power (P_{sd})	0.45 µW	0.032 µW	1.53 µW
Data acquisition (E_{acq})	0.53 µJ	–	4.67 µJ
Wake-up energy ($E_{\text{sd,stdby}}$)	–	19.5 µJ	45.9 µJ
Packet transmission[2] from:			
Standby ($E_{\text{pckt,stdby}}$)	50 µJ (avg)	116 µJ	118 µJ
Shutdown ($E_{\text{pckt,sd}}$)		106 µJ	108 µJ

[1] With SRAM data retention.
[2] BLE packet with a 9-byte (resp. 14-byte) payload transmitted at 6 dBm (resp. 5 dBm) on one channel for the STM32WB55 (resp. CC2650) MCU.

room, depicted in Fig. 7(a). When motion is detected, a BLE packet is immediately transmitted to the gateway to indicate the room is occupied. The MCU then goes back to motion detection mode and starts the timer for the back-off time. If during any of the following data acquisitions, until the end of the back-off time, a motion is again detected, then the timer is restarted. If instead, no motion is detected, then a packet is transmitted to the gateway indicating the room is no longer occupied.

The worst-case scenario thus happens when a packet is transmitted immediately after one back-off time, in which case the average power consumption can be computed as

$$P_{\text{WC}} = P_{\text{detect}} + \frac{2 \cdot E_{\text{pckt,stdby}}}{T_{\text{bo}}}, \tag{5}$$

where T_{bo} is the back-off time and $E_{\text{pckt,stdby}}$ is the energy needed to transmit a packet after waking up from standby, including the energy necessary for the MCU to wake up from the standby mode. It can be noted that it is limited by the power consumed during motion detection and therefore by P_{stdby}. Fig. 8 shows the power consumption according to (5) in the worst-case scenario as a function of T_{bo}. It was calculated from the performance of the CC2650 as reported in [6], available in Table I. For a sampling frequency of 1 S/s and a back-off time of 1 min, the average power consumption in the worst-case scenario is 6.2 µW. It is above the target consumption, mainly because the standby power of the CC2650 is already equal to the target power consumption, as shown in Table I. Therefore, another MCU with lower standby power must be used in order to achieve the target of 4 µW. The STM32WB55 MCU from STMicroelectronics [26] was chosen as a replacement because its standby power is 4 to 6× lower than that of the CC2650. Its specifications are also shown in Table I for comparison.

Fig. 8 also shows the worst-case power consumption when using the STM32WB55 MCU for two different f_{S}. When considering 1 S/s of sampling frequency similarly to the previous MCU, a deterioration of the performance is noticed because of the higher energy needed for an ADC acquisition. Even if the new MCU has a lower standby power, it has significantly higher wake-up energy, which increases the average power consumption during motion detection, i.e., 5.75 µW. As a consequence, even if the back-off time is increased infinitely, it is not possible to reach the power consumption target. If the

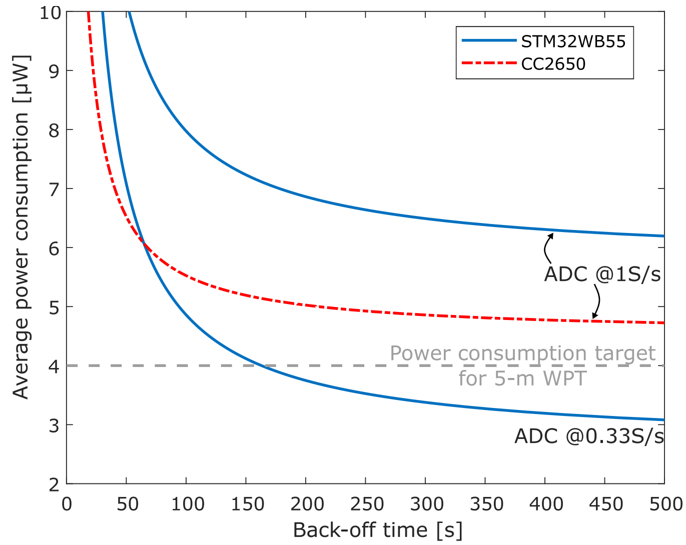

Fig. 8. Average power consumption in the worst-case scenario for Strategy A. The performance of the CC2650 [25] MCU is compared to two configurations of the STM32WB55 [26].

sampling frequency is decreased to 0.33 S/s, which would degrade the system responsiveness, the motion detection power goes down to 2.64 µW. However, a back-off time of almost 3 min is needed for the worst-case consumption to be also below the target, impacting even further the system responsiveness. In this case, the high wake-up energy limits the worst-case average power by increasing the energy needed for packet transmission. Both issues can only be solved by using an alternative strategy.

B. Strategy B: Always-on Sensing with Event-driven MCU Wake-up

The objectives of this new strategy are therefore to minimize the number of times the MCU must wake up from sleep mode to control the system and to decrease the number of packets transmitted. Both objectives have the goal of reaching the target power consumption with the STM32WB55, taking advantage of its very low standby power.

Firstly, the periodic wake-up strategy is changed to an event-driven wake-up. More specifically, this means that the signal processing for motion detection is transferred from the MCU to the AFE, which now will function in an always-on approach during motion detection, generating an interrupt request (IRQ) to wake up the MCU when a movement is detected. When managing the IRQ, the MCU turns off the AFE to save power.

Secondly, the communication scheme is changed to the one shown in Fig. 7(b). After a system reset, the AFE stays on for motion detection while the MCU is in sleep. It can go to the deepest sleep mode because the RTC is not needed. In this mode, called shutdown mode for both MCUs considered here, the power consumption of the MCU (P_{sd}) is negligible in comparison to that of the AFE. When a motion is detected, the MCU is woken up by an IRQ generated by the AFE and transmits a BLE packet to alert the gateway of movement in the room. Then, the system starts the back-off time, during which the AFE is turned off and the MCU is in standby mode to keep track of time with the RTC. Once over, the MCU

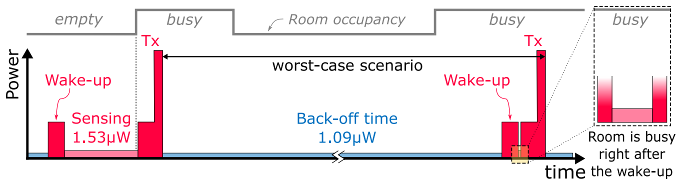

Fig. 9. Power profile of the smart sensor for Strategy B. The worst-case scenario is shown, corresponding to a movement detected exactly after one back-off time.

must wake up to return the system to the state after reset. On the gateway side, the room is considered again unoccupied if no packet is received after a certain amount of time. This time consists of the back-off time plus a small time margin that allows the system to start up completely and to detect if the room is unoccupied, e.g., for a back-off time of 50 s, the gateway considers the room is again unoccupied if it does not receive a new packet after 60 s.

To enhance the reliability of the communication scheme, an acknowledgment system similar to the one used in [6] is implemented. By leveraging the scannable advertisements of the BLE protocol, the smart sensor can know whether the gateway received its broadcast packets thanks to the scan requests. In the case where the smart sensor does not receive the corresponding scan request from the gateway, it repeats the transmission a maximum of two times to guarantee that a minimum of packets are lost. In order to keep the average power consumption constant, even after three trials, the back-off time is adapted and becomes longer to compensate for the extra energy consumed for the additional packet transmission.

The average power consumption during motion detection, in this case, can be approximated to the power of the AFE because the shutdown power of the MCU can be neglected, especially for the STM32WB55 whose shutdown power is more than 60× lower than the AFE power. On the other hand, the worst-case scenario for the power consumption changes with this strategy and corresponds to the case when a motion is detected immediately after the back-off time, as shown in Fig. 9. This power consumption can be computed as

$$P_{\text{WC}} = P_{\text{stdby}} + \frac{E_{\text{pckt,sd}} + E_{\text{sd,stdby}}}{T_{\text{bo}}}, \quad (6)$$

where $E_{\text{pckt,sd}}$ and $E_{\text{sd,stdby}}$ are the energies necessary to transmit a packet after waking up from shutdown and to change from standby to shutdown mode, respectively.

Fig. 10 shows the power consumption for the worst-case scenario for both MCUs, along with the AFE power consumption in dashed lines. As the power with the CC2650 is still limited by the MCU standby power, as can be seen in (6), the CC2650 cannot achieve the targeted power consumption. On the contrary, the STM32WB55 does reach it with an acceptable back-off time of 60 s. The figure also shows the average power consumption when multiple trials of the packet transmission are performed, with an emphasis on the adaptive nature of the back-off time.

A final degree of freedom consists of the number of advertising channels to use for transmitting the BLE beacon. The Bluetooth standard suggests the repetition of the broadcast packet in the three advertising packets, demanding higher energy because of this repetition. Nevertheless, as seen in

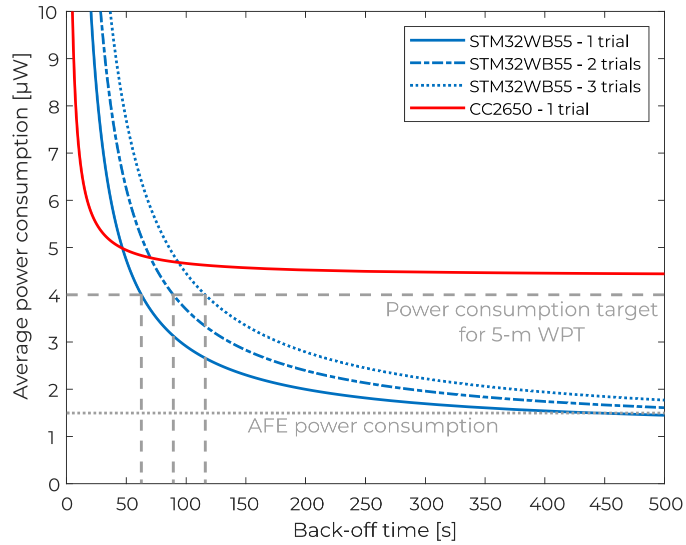

Fig. 10. Average power consumption in the worst-case scenario for Strategy B. The vertical dashed lines show the adaptive back-off time implemented to maintain a constant average power consumption even after multiple transmission trials.

TABLE II
ENERGY COMPARISON FOR DIFFERENT NUMBERS OF PACKETS AND FOR DIFFERENT NUMBERS OF ADVERTISING CHANNELS.

Advertising channels	Energy for one trial	Energy for three trials
Only one	118 µJ	246 µJ
All three	130 µJ	293 µJ

Table II, the increment is not linear with the number of transmitted packets mainly because this energy also includes the MCU wake-up and software initialization that is performed only once. It represents an increment of only 19 % for three times more packets sent. This translates into an increment of the back-off time of 10 s in average to maintain an average power of 4 µW, which does not represent a significant degradation in the system performance for the targeted application but allows greater compatibility since most BLE devices use the three advertising channels.

C. Sensor Interface

The use of Strategy B with always-on sensing directly impacts the design of the AFE, which is not only in charge of conditioning the signal coming from the PIR sensor but also of detecting movements in the room. Fig. 11 shows the schematic of the AFE, which is based on the application note of Texas Instruments [27]. It includes an active band-pass filter, followed by a window comparator that converts its analog output to digital signals which indicate when a motion is detected. These digital signals generate an IRQ on the MCU, triggering a BLE packet transmission.

Since the AFE remains always-on during motion detection, the TLV8801 amplifier [28] was chosen for the operational amplifier in the filter and the TLV3691 comparator [23] for the two comparators because both components have an ultra-low power consumption. In addition, three modifications to the original design from [27] are introduced. The first two are inspired by [6] and consist in removing an additional stage

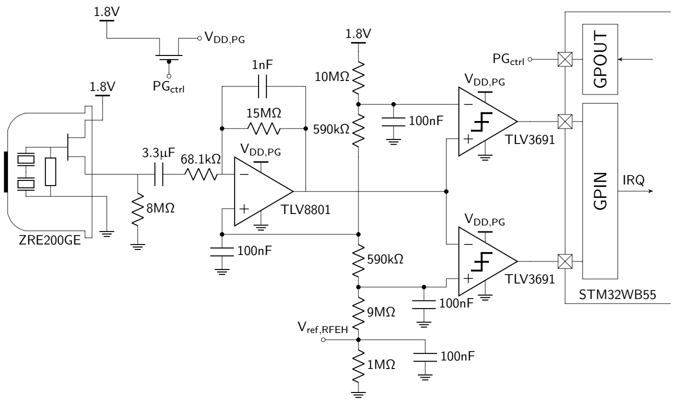

Fig. 11. Analog front-end schematic.

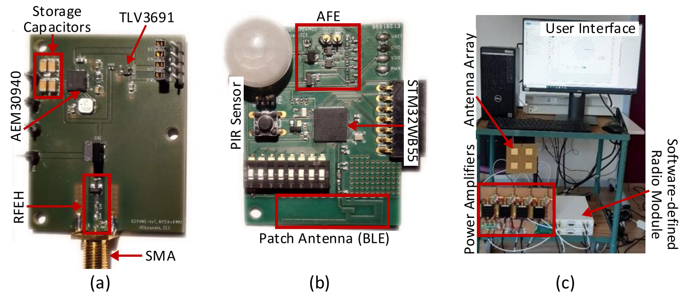

Fig. 12. Stackable PCBs for (a) the harvesting subsystem and (b) the sensing subsystem. The SMA connector serves to connect the energy harvesting antenna. (c) Remote power head.

of active filtering, which is not strictly required and can be removed to save power; and in increasing the source resistance of the PIR resistor, which decreases the power consumption of the sensor without a significant impact on the signal-to-noise ratio [6]. The third modification is a direct consequence of the first one. As a gain stage was removed, the amplitude of the signal was decreased and the thresholds of the window comparator had to be reduced to maintain the sensibility. There is however a limit on the size of the comparison window, as it needs to be large enough to avoid false positives due to the sensor or environmental noise, and the comparator offset.

The amplifier and comparators are power gated during the back-off time to save power, an operation that is controlled by the MCU through the GPIOs by changing the gate voltage of a PMOS transistor. The transducer, however, is not power gated to avoid its long start-up time at each wake-up [6].

V. Prototyping and Global Performance

The system prototype is shown in Fig. 12. The smart sensor was implemented on stackable printed circuit boards (PCBs), one per subsystem. A practical problem that needs to be addressed when testing prototypes of this type of system concerns the cold start of the smart sensor. The design and optimization of the system discussed in the previous sections consider only the steady-state operation of the smart sensor. However, when the supply voltage first appears and all the components of the sensing subsystem initialize at the same time, there is a peak in the consumption of the smart sensor, as shown in the current trace in Fig. 13. The power consumption of the smart sensor is temporarily increased and therefore, the operation at the maximum theoretical distance can no longer be achieved. This problem can simply be solved by decreasing the distance between the smart sensor and the RPH. To limit this loss in distance, the transmitted power was boosted by 5 dB during the cold start only. Even though this boost risks violating the EIRP regulations, it is acceptable if the absence of human presence is guaranteed. The whole system was tested successfully from the cold start at 3.5 m of separation between the RPH and the smart sensor.

The performance of the WPT system can be evaluated using the PTE computed from (3). At 5 m, where the path loss is 31.4 dB and the PHE is 20.44 %, a total of 4.66 µW can be harvested. Considering only the power amplifiers for the PTXE, since the software-defined radio modules used for the rest of the RPH are not designed to be power efficient, the PTE is 427 ppb, or equivalently 427 nW/W, given that the used power amplifiers from TriQuint [19] have an efficiency of 1.16 %. However, the power amplifiers are not optimized either in this system. State-of-the-art power amplifiers working with signals with PAPR can reach an efficiency of 45 % [29]. Therefore, optimizing the power amplifiers to have such efficiency would increase the PTE to maximum 17 ppm, or 17 µW/W.

VI. Life-cycle Assessment

Given the current environmental situation of the Anthropocene and the upcoming massive deployment of smart objects, it becomes critical to question the environmental relevance of technological innovations, especially when they embed electronic components as they are known to be resource- and energy-intensive to produce [30]. An LCA can help in this matter as it is a standardized methodology to evaluate the environmental impacts over multiple indicators [31]. In order to compare the environmental performance of the WPT solution to its battery-powered equivalent, a comparative cradle-to-grave LCA was carried out including life-cycle phases from raw material extraction and production to use phase and end of life (EoL). The usage of networks and the cloud were not taken into account as they are not necessary for this application. The environmental impacts were modeled with the GaBi LCA software tool using the ReCiPe 2016 midpoint (H) method. Four indicators were considered, namely primary energy demand (PED), global warming potential (GWP), terrestrial ecotoxicity (EcoTox), and freshwater consumption (Water). The functional unit is defined as *one system over a 10-year lifetime*, where the *system* can be either the WPT room-occupancy tracking version as presented in Fig. 1 or its battery-powered equivalent where the harvesting subsystem is replaced by a coin cell and no RPH is used at the base station.

For the bill of material (BoM) and the life cycle inventory (LCI), optimized systems were assumed in order to avoid a bias for the WPT as a development prototype is undeniably under-optimized in terms of hardware design and performance. A streamlined BoM for both versions is given in Table III. The RPH was included in the BoM because the need for specialized hardware and the limited allowed distance between the RPH and the smart sensors do not allow the reuse of existing Wi-Fi or Bluetooth infrastructure. As the information gateway could

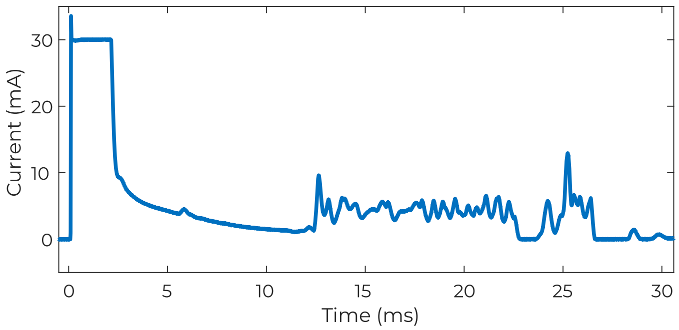

Fig. 13. Current trace of the cold start of the sensing subsystem of the smart sensor. The spurious activity of high power consumption present during the cold start prevents the achievement of the theoretical separation between the smart sensor and the RPH.

be deployed with the smart sensors or integrated into the existing infrastructure, its impact is reported separately from that of the RPH. For the production phase, the GaBi professional and GaBi Extension XI (Electronics) databases [32] were used to model the different electronic components of the two versions. The environmental impacts related to the production of the battery have been attributed to the use phase of the smart sensor and thanks to its very low power consumption of 4 µW, a single 3 V 120 mAh lithium poly-carbonmonofluoride coin cell is sufficient to power up the smart sensor over its lifetime. The ratio between the PED for the production of this coin-cell battery and its capacity is around 100-150× [32], which is similar to what is used in [33]. For the use phase, the EU-28 electricity grid mix was used for the base station. The power consumption at the RPH is assumed to be proportional to the number of smart sensors, which is a reasonable first-order approximation. However, the power consumption of the gateway is considered to be similar regardless of the number of smart sensors, i.e., $P_{\text{avg}} = 50\,\text{mW}$. For the EoL, a basic model was considered by assuming that electronic parts would end up in an incineration plant and plastic parts in a landfill. All data and specific assumptions used in this analysis are provided as supplementary material.

Fig. 14 shows the results of the LCA. For each version, two scenarios were analyzed: the first scenario combines one single smart sensor with one base station whereas in the second scenario one base station is shared between 8 smart sensors. This scenario is likely to be more representative of a real-life deployment and corresponds to the limit of smart sensors that can be supplied by a single RPH for the 64-tone custom high-PAPR waveform used, as described in Section III. In the single-sensor scenario, the environmental impacts are balanced between the production and the use phase, both for the WPT and for the battery-powered version. Nevertheless, the WPT version yields higher absolute impacts, i.e., from 5.5 to 6.3× depending on the considered indicator. In the 8-sensor scenario, the use phase dominates by more than 68 % in the WPT version. This is explained by the high RPH power consumption of 1.88 W. Results show that increasing the number of smart sensors generally strengthens the previous conclusions, with impacts up to 10.3× higher for the WPT version. In both scenarios, the production dominates the EcoTox indicator by at least 92 %, mainly due to PCB and integrated circuits (IC).

TABLE III
STREAMLINED BILL OF MATERIAL (BOM) FOR THE LCA OF BATTERY-POWERED AND WPT-POWERED SYSTEMS.

Part	Quantity	Units	Description
Common components			
Gateway	1		$P_{\text{avg}} = 50\,\text{mW}$
PCB	50	cm^2	HASL FR4 4 layers
Relay	1	piece	–
External antenna	1	piece	Whip-like antenna
Crystal	2	piece	–
AC/DC power supply†	1	piece	–
ICs$^\triangleright$ (+ package)	12	mm^2	STM32WB55
LED	1	piece	–
Others⋆			
Smart sensor	1–8		Power budget = 4 µW
PCB	20	cm^2	HASL FR4 2 layers
ICs$^\triangleright$ (+ package)	12	mm^2	STM32WB55
Comparator	2	piece	TLV3691
Transistor	1	piece	PMOS
Operational amplifier	1	piece	TLV8801
PIR sensor$^\diamond$	1	piece	ZRE200GE
Plastic lens	2	g	–
Others⋆			
Supply - Battery version	1–8		
PCB	10	cm^2	HASL FR4 2 layers
Coin-cell battery	1	piece	3V 120mAh Li
LDO	1	piece	–
Supply - WPT version			
RPH	1		$P_{\text{TX,in}} = 235\,\text{mW}$ (PTE = 17 µW/W)
PCB	400	cm^2	HASL FR4 4 layers
PCB antennas array	400	cm^2	HASL FR4 2 layers
ICs$^\triangleright$ (+ package)	24	mm^2	Real-time MCU (w. DSP)
Power amplifier	4	piece	TPQ9111-like (efficiency = 45 %)
Crystal	1	piece	–
AC/DC power supply†	1	piece	–
RFEH	1–8		
PCB	10	cm^2	HASL FR4 2 layers
PCB double-patch antenna	48	cm^2	HASL FR4 2 layers
ICs$^\triangleright$ (+ package)	6	mm^2	AEM30940
Comparator	1	piece	TLV3691
Power inductor	1	piece	–
Storage capacitor	4	piece	220 µF
Others⋆			

⋆: includes passive components (e.g., capacitors, resistors, inductors, EMS shield, press button, SnAgCu solder paste, diodes, ...), transistors, and filter
†: includes power transistors, ring core coil, diodes and other passive components, connectors and cables
▷: CMOS good die area (die-to-package approx.) ⋄: CMOS approx.

The impacts associated with the production of the battery are orders of magnitude smaller than for the other parts, which explains why it cannot be seen easily in Fig. 14. For the four indicators considered in this study, it is clear that the environmental impacts of the WPT version over a 10-year lifetime are significantly higher than the battery-powered equivalent.

However, although the proposed WPT system has already been optimized, it is likely not representative of all WPT systems. Indeed, other systems could have a better PTE, allow for connecting a higher number of sensors, use manufacturing techniques that are more environmentally friendly such as additive manufacturing, or even propose a more integrated design. We, therefore, analyze the sensitivity of our LCA conclusions for a generalized WPT system WPT^g, as defined in Fig. 15. Four parameters are considered in this sensitivity analysis, namely (i) the number of smart sensors N_{sensors} in the system, (ii) the PTE of the WPT^g system, (iii) an improvement factor F_{core} regarding the impacts of the PCB for the core electronics $I_{\text{PCB, core}}$, and (iv) an improvement factor F_{ant} regarding the impacts of the PCB for the antennas of the RFEH and RPH, $I_{\text{PCB, antennas EH}}$ and $I_{\text{PCB, antennas RPH}}$ respectively. All

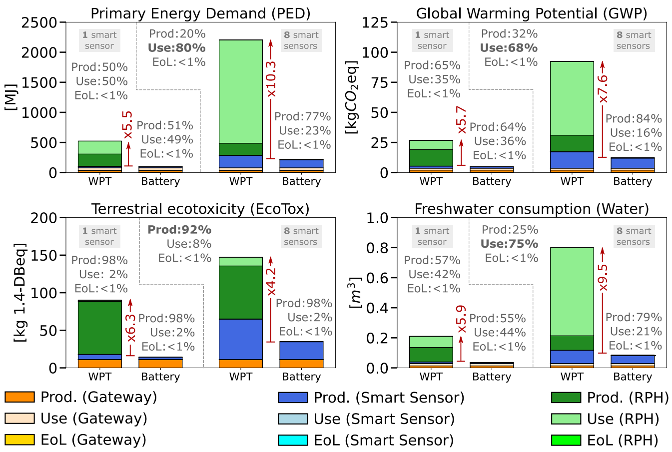

Fig. 14. LCA results. Percentages give the share of production, use, and end of life (EoL) for each result.

data used in this sensitivity analysis are available in the supplementary material. The results of the sensitivity analysis are presented in Figs. 15(a)-(d), depicting the ratio between the impacts of the WPT and the battery-powered systems. The effect of improving either the PTE to its maximum possible value or the manufacturing of PCB for the antennas by a factor 100 [34], [35] is shown in Figs. 15(b)-(c) while the effect of combining both improvements is illustrated in Fig. 15(d). With these improvements, the environmental impacts of the WPT^g system are almost equivalent to the battery-powered system, especially for a higher number of nodes as the RPH is amortized. Yet, the WPT^g system remains more impacting and the absolute impacts increase with the number of sensors, as shown in Fig. 15(d). Moreover, as shown clearly in (3), a PTE equal to 1 is unrealistic in practice, although it is considered here as a theoretical boundary. Furthermore, increasing significantly the PTE would also require extra hardware in order to improve TX and RX efficiency, which is not captured in this analysis. The effect of F_{core} was also investigated and it does not improve the situation as both systems benefit from the reduction of the impacts. The inclusion or exclusion of the gateway does not change the conclusions either as it is used in both systems. More details on both analyses are provided in the supplementary material. Finally, the environmental impacts of the components ($I_{\text{components}}$) were reduced by considering further optimizations such as die area reduction (-50%) for the IC of the RPH. This sensitivity analysis supports the generalization of our LCA conclusions beyond the proposed system. Consequently, WPT may be acceptable for applications where this is the only possible solution but it must not become a widespread standard to power smart sensors as the overall environmental footprint of the system is increased. It also means that upcoming WPT research or products cannot be called "green" just because they avoid the use of batteries. This highlights again the critical need to carry out systematic LCAs for IoT devices [30].

A brief discussion can provide perspectives on these conclusions. First, changing the energy mix can have an impact on the results, especially for the GWP and Water indicators. For instance, if the Chinese energy mix is used for powering up the base station instead of the EU-28 energy mix, GWP results in the 8-sensor scenario increase up to +80 % and +16 % for the

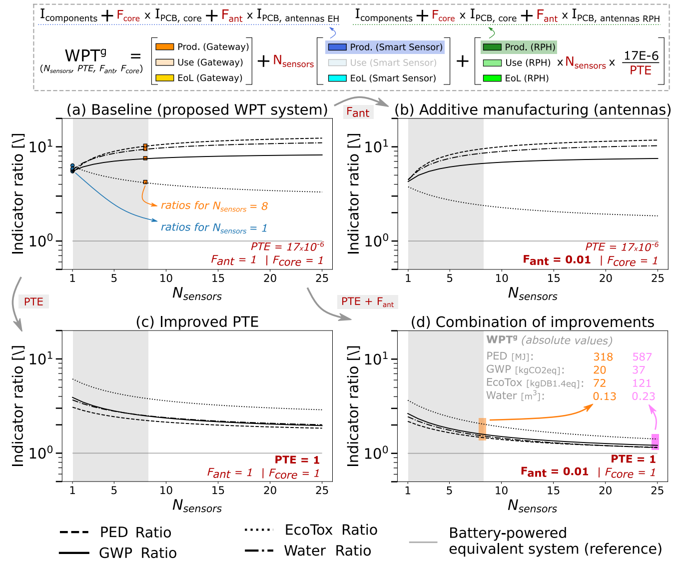

Fig. 15. Sensitivity analysis and generalization for WPT systems. The evolution of the ratio between the impacts of the WPT and the battery-powered equivalent systems is provided for each of the four indicators under study.

WPT and battery version, respectively. Then, a deeper analysis could take into account the fact that the effective lifetime of a battery could be shorter than its nominal specifications due to thermal stress or aging phenomena, for instance. Although this will not change the conclusions, the gaps between the two versions will shrink if heavy maintenance is needed, e.g., the replacement of the whole smart sensor rather than only the battery. Finally, the end-of-life of the battery could be better modeled as the environmental impacts generated by specific recycling processes are not captured here.

VII. Conclusion

In this paper, we focused on the design of a state-of-the-art 2.45-GHz SWIPT system to determine its technical and ecological limits to supply battery-less smart sensors, particularly in comparison with battery-powered sensors. The system was designed to maximize the achievable separation between the smart sensor and the RPH, estimated to be 5 m. This required the optimization of all the parts of the system: on the RPH, the implementation of a beamforming protocol allowing to maximize the total harvested power; and on the smart sensor, the choice of MCU and motion detection strategy allowing to operate under the strong power consumption constraint of 4 µW. The system was successfully tested at a distance of 3.5 m between the RPH and the smart sensor, including the cold start of the latter. This starting sequence must not be overlooked in the system design as it was the critical point preventing the system from reaching a 5-m supply distance. Finally, this work demonstrates the importance of carrying out a specific LCA for the design of IoT smart sensors. Indeed, our LCA results show that the environmental impacts of the WPT system were higher than the battery-powered ones, up to a factor 10.3× for the deployment scenario with several smart sensors. A parametric sensitivity analysis also demonstrated the stability of our conclusions even with (i) an increasing number of smart sensors, (ii) significant improvements in terms of

PTE, (iii) the use of advanced manufacturing techniques such as printed electronics for PCB. As these findings may seem counterintuitive because primary batteries are usually associated with a high environmental impact, this work calls for the systematic use of LCA in the context of IoT.

ACKNOWLEDGMENTS

This work was supported by the Brussels Institute for Research and Innovation (INNOVIRIS) under the COPINE-IoT project, the Fonds européen de développement régional (FEDER) and the Wallonia within the Wallonie-2020.EU program.

REFERENCES

[1] Statista. (2016) Number of IoT devices 2015-2025. Accessed: Feb., 2022. [Online]. Available: https://www.statista.com/statistics/471264/iot-number-of-connected-devices-worldwide/

[2] Cisco. (2020) Cisco Annual Internet Report - Cisco Annual Internet Report (2018–2023) White Paper. Accessed: Feb., 2022. [Online]. Available: https://www.cisco.com/c/en/us/solutions/collateral/executive-perspectives/annual-internet-report/white-paper-c11-741490.html

[3] Haltian. Thingsee presence. Accessed: Feb., 2022. [Online]. Available: https://haltian.com/product/thingsee-presence/

[4] Flexicount. Live Occupancy Solution. Accessed: Feb., 2022. [Online]. Available: https://flexicount.com/occupancy-sensor

[5] Leviton. Occupancy and Vacancy Sensors. Accessed: Feb., 2022. [Online]. Available: https://www.leviton.com/en/products/commercial/lighting-controls/occupancy-sensors-and-vacancy-sensors

[6] R. Dekimpe, P. Xu, M. Schramme, P. Gérard, D. Flandre, and D. Bol, "A battery-less BLE smart sensor for room occupancy tracking supplied by 2.45-GHz wireless power transfer," *Integration*, vol. 67, pp. 8–18, Jul. 2019.

[7] L.-G. Tran, H.-K. Cha, and W.-T. Park, "RF power harvesting: A review on designing methodologies and applications," *Micro and Nano Syst. Lett.*, vol. 5, no. 14, Dec. 2017.

[8] S. K. Divakaran, D. D. Krishna, and Nasimuddin, "RF energy harvesting systems: An overview and design issues," *Int J RF Microw Comput Aided Eng*, vol. 29, no. 1, p. e21633, Jan. 2019.

[9] M. Wagih, A. S. Weddell, and S. Beeby, "Rectennas for Radio-Frequency Energy Harvesting and Wireless Power Transfer: A Review of Antenna Design [Antenna Applications Corner]," *IEEE Antennas Propag. Mag.*, vol. 62, no. 5, pp. 95–107, Oct. 2020.

[10] G. Paolini, D. Masotti, M. Guermandi, M. Shanawani, L. Benini, and A. Costanzo, "An Ambient-Insensitive Battery-Less Wireless Node for Simultaneous Powering and Communication," in *2020 50th Eur Microw Conf (EuMC)*. IEEE, Jan. 2021, pp. 522–525.

[11] M. Pizzotti, L. Perilli, M. del Prete, D. Fabbri, R. Canegallo, M. Dini, D. Masotti, A. Costanzo, E. Franchi Scarselli, and A. Romani, "A Long-Distance RF-Powered Sensor Node with Adaptive Power Management for IoT Applications," *Sensors*, vol. 17, no. 8, Jul. 2017.

[12] H. Abbasizadeh, S. Y. Kim, B. Samadpoor Rikan, A. Hejazi, D. Khan, Y. G. Pu, K. C. Hwang, Y. Yang, D. I. Kim, and K.-Y. Lee, "Design of a 900 MHz Dual-Mode SWIPT for Low-Power IoT Devices," *Sensors*, vol. 19, no. 21, Oct. 2019.

[13] K. W. Choi, S. I. Hwang, A. A. Aziz, H. H. Jang, J. S. Kim, D. S. Kang, and D. I. Kim, "Simultaneous Wireless Information and Power Transfer (SWIPT) for Internet of Things: Novel Receiver Design and Experimental Validation," *IEEE Internet Things J.*, vol. 7, no. 4, pp. 2996–3012, Apr. 2020.

[14] J. Kim, B. Clerckx, and P. D. Mitcheson, "Experimental Analysis of Harvested Energy and Throughput Trade-off in a Realistic SWIPT System," in *2019 IEEE Wireless Power Transfer Conference (WPTC)*. London, United Kingdom: IEEE, Jun. 2019.

[15] e-peas, "Highly efficient, regulated dual-output, ambient energy manager for AC or DC sources with optional primary battery," AEM30940 Datasheet, 2020.

[16] Zilog, "ZMOTION pyroelectric sensors," ZRE200GE Datasheet, 2014.

[17] National Instruments, "Software Defined Radio Reconfigurable Device," USRP-2944 Datasheet, 2017.

[18] P. Xu, D. Flandre, and D. Bol, "A Self-Gating RF Energy Harvester for Wireless Power Transfer With High-PAPR Incident Waveform," *IEEE J. Solid-State Circuits*, vol. 56, no. 6, pp. 1816–1826, Jun. 2021.

[19] TriQuint Semiconductor, "TQP9111 1.8-2.7 GHz 2 Watt Power Amplifier," TPQ9111 Datasheet, Sep. 2015.

[20] P. Xu, D. Flandre, and D. Bol, "Analysis and Design of RF Energy-Harvesting Systems with Impedance-Aware Rectifier Sizing," *IEEE Trans. Circuits Syst. II*, 2022.

[21] ——, "Analysis, Modeling, and Design of a 2.45-GHz RF Energy Harvester for SWIPT IoT Smart Sensors," *IEEE J. Solid-State Circuits*, vol. 54, no. 10, pp. 2717–2729, Oct. 2019.

[22] S.-E. Adami, P. Proynov, G. S. Hilton, G. Yang, C. Zhang, D. Zhu, Y. Li, S. P. Beeby, I. J. Craddock, and B. H. Stark, "A Flexible 2.45-GHz Power Harvesting Wristband With Net System Output From -24.3 dBm of RF Power," *IEEE Trans. Microwave Theory Techn.*, vol. 66, no. 1, pp. 380–395, Jan. 2018.

[23] Texas Instruments, "TLV3691 0.9-V to 6.5-V, Nanopower Comparator," TLV3691 Datasheet, 2015.

[24] L. Liu, R. Zhang, and K.-C. Chua, "Multi-Antenna Wireless Powered Communication With Energy Beamforming," *IEEE Trans. Commun.*, vol. 62, no. 12, pp. 4349–4361, Dec. 2014.

[25] Texas Instruments, "SimpleLink multistandard wireless MCU," CC2650 Datasheet, 2016.

[26] STMicroelectronics, "Multiprotocol wireless 32-bit MCU Arm-based Cortex-M4 with FPU, Bluetooth 5 and 802.15.4 radio solution," STM32WB55 Datasheet, 2020.

[27] Texas Instruments, "Ultra-low-power wireless PIR motion detector for cost-optimized systems reference design," TIDA-01398 Application Note, 2017.

[28] ——, "TLV8801/TLV8802 320 nA Nanopower Operational Amplifiers fors Cost-Optimized Systems," TLV8801 Datasheet, 2016.

[29] P. A. Godoy, S. Chung, T. W. Barton, D. J. Perreault, and J. L. Dawson, "A 2.4-GHz, 27-dBm Asymmetric Multilevel Outphasing Power Amplifier in 65-nm CMOS," *IEEE J. Solid-State Circuits*, vol. 47, no. 10, pp. 2372–2384, Oct. 2012.

[30] T. Pirson and D. Bol, "Assessing the embodied carbon footprint of IoT edge devices with a bottom-up life-cycle approach," *J Cleaner Prod*, vol. 322, Nov. 2021.

[31] ISO, 14040:2006, *Environmental management – Life cycle assessment – Principles and framework*, 2006.

[32] Sphera. (2021) GaBi extension database XI : Electronics. Accessed: Dec. 2021. [Online]. Available: http://www.gabi-software.com/international/databases/gabi-databases/electronics/

[33] M. Friedli, L. Kaufmann, F. Paganini, and R. Kyburz, "Energy Efficiency of the Internet of Things," Technol and Energy Assessment Rep Prepared for IEA 4E EDNA, 2016.

[34] J. Liu, C. Yang, H. Wu, Z. Lin, Z. Zhang, R. Wang, B. Li, F. Kang, L. Shi, and C. P. Wong, "Future paper based printed circuit boards for green electronics: Fabrication and life cycle assessment," *Energy Environ. Sci.*, vol. 7, no. 11, pp. 3674–3682, 2014.

[35] M. N. Nassajfar, I. Deviatkin, V. Leminen, and M. Horttanainen, "Alternative materials for printed circuit board production: An environmental perspective," *Sustainability*, vol. 13, no. 21, p. 12126, Nov. 2021.

Marco Gonzalez (Student Member, IEEE) received the M.Sc. degree (cum laude) in Electrical Engineering from the Université catholique de Louvain (UCLouvain), Louvain-la-Neuve, Belgium, in 2019, where he is currently pursuing a Ph.D. degree in microelectronics, under the supervision of Prof. David Bol. His current research includes the design of low-power analog, mixed-signal, and radio-frequency integrated circuits.

Pengcheng Xu (Member, IEEE) received the bachelor's degree (Hons.) in physics from Shanghai Normal University, Shanghai, China, in 2013, the master's degree (Hons.) in integrated circuit engineering from Tongji University, Shanghai, in 2016, and the Ph.D. degree in electrical engineering from the Université catholique de Louvain (UCLouvain), Louvain-la-Neuve, Belgium, in 2021. In 2015, he was an Exchange Student at the University of Erlangen-Nuremberg, Erlangen, Germany.

His research area includes analog and mixed-signal integrated circuit design. From February 2017 to November 2020, he was a Research Assistant in electrical engineering with UCLouvain. Since November 2020, he is a Research Associate with the Department of Circuits and Systems, Fraunhofer EMFT, Munich, Germany. He was the Holder of the Chinese National Scholarship three times. He has authored or co-authored more than ten technical articles, including JSSC, ISSCC, ASSCC, TCAS-II, and Internet of Things Journal. He holds one delivered European patent.

He is also a Member of IEEE Solid-State Circuits Society. He was a recipient of the Shanghai Outstanding Graduates Student Award in 2013 and 2016, the Meritorious Winner in the 2013 Mathematical Contest in Modeling of America (MCM) and Chinese government award for outstanding self-finance students abroad in 2020. He also serves as a Reviewer for various journals and conferences, such as the TCAS-I/II, IEEE WIRELESS COMMUNICATIONS LETTERS, and IEEE ACCESS. He is a TPC member of the 2022 and 2023 IEEE Design Automation Conference.

Rémi Dekimpe received the M.Sc. degree in Biomedical Engineering in 2017 and Ph.D. degree in Engineering Science in 2022 from UCLouvain, Belgium. He is now a postdoctoral researcher in the Electronic Circuits and Systems group in UCLouvain under the supervision of Prof. David Bol. His current research focuses on mixed-signal IC design, ultra-low-power smart sensors for biomedical applications, and the impacts of information and communication technologies on socio-environmental sustainability.

Maxime Schramme received the M.Sc. degree in Electrical Engineering and the Ph.D. degree in microelectronics from UCLouvain, Louvain-la-Neuve, Belgium, in 2016 and 2022, respectively. He fully exploits the back-gate biasing capability of FD-SOI technology to reduce power, increase circuit speed, ensure good performance and/or compensate process-voltage-temperature variations. In this context, his current research focuses on the design of ultra-low-power clock generation and frequency synthesis.

Ivan Stupia (Member, IEEE) is research associate at the University of Louvain, Belgium. He began his career at the University of Pisa, Italy, where he received the PhD degree in 2009. In 2011 he joined the Institute of Information and Communication Technologies, Electronics and Applied Mathematics (ICTEAM) of the University of Louvain. His expertise and general interests span the areas of wireless communications and signal processing with special emphasis on application of advanced mathematical tools to the design of self-adaptive/self-organizing wireless networks, energy harvesting, multi-function RF systems, and green and cost-effective design of wireless networks. His academic experience is corroborated by more than 50 publications in international journals and proceedings of international conferences. He was involved in various European and national projects on wireless communications in different fields of application (cellular systems, wireless sensor networks, security and aeronautical communications).

Thibault Pirson received the M.Sc. degree in Electrical Engineering in 2019 from UCLouvain, Belgium. Since, he is a Ph.D. researcher in the Electronic Circuits and Systems group at UCLouvain under the supervision of Prof. David Bol. His current research focuses on LCA of electronics, and more specifically LCA of Internet-of-Things (IoT) devices. He is mainly interested in the development of information and communication technologies within planetary boundaries and he co-founded the Sustainable ICT (SICT) doctoral summer school in 2020.

David Bol (Senior Member, IEEE) received the Ph.D. degree in engineering science from UCLouvain, Louvain-la-Neuve, Belgium, in 2008, in the field of ultra-low-power digital nanoelectronics. In 2005, he was a Visiting Ph.D. Student at CNM, Seville, Spain, and in 2009, he was a Post-Doctoral Researcher at intoPIX, Louvain-la-Neuve. In 2010, he was a Visiting Post-Doctoral Researcher at the UC Berkeley Laboratory for Manufacturing and Sustainability, Berkeley, CA, USA.

In 2015, he has participated to the creation of e-peas semiconductors spin-off company. He is currently an Associate Professor at UCLouvain. He leads the Electronic Circuits and Systems (ECS) Group focused on ultra-low-power design of integrated circuits for environmental and biomedical IoT applications including computing, power management, sensing, and wireless communications. He is actively engaged in a social-ecological transition in the field of ICT research with a post-growth approach. He has authored more than 150 papers and conference contributions and holds three delivered patents.

Prof. Bol (co-)received four Best Paper/Poster/Design Awards in IEEE conferences (ICCD 2008, IEEE International SOI Conference 2008, FTFC 2014, and ISCAS 2020) and supervised the Ph.D. thesis of Charlotte Frenkel who received the 2021 Nokia Bell Scientific Award and the 2021 IBM Innovation Award for his Ph.D. He serves as a reviewer for various IEEE journals and conferences and presented several keynotes in international conferences.